



---

## Polyphenol-Induced Adhesive Liquid Metal Inks for Substrate-Independent Direct Pen Writing

AUTHOR(S)

M A Rahim, F Centurion, J Han, R Abbasi, M Mayyas, J Sun, M J Christoe, D Esrafilzadeh, F M Allieux, M B Ghasemian, J Yang, J Tang, T Daeneke, S Mettu, Jin Zhang, M H Uddin, R Jalili, K Kalantar-Zadeh

PUBLICATION DATE

03-03-2021

HANDLE

[10536/DRO/DU:30147420](https://hdl.handle.net/10536/DRO/DU:30147420)

Downloaded from Deakin University's Figshare repository

Deakin University CRICOS Provider Code: 00113B

# Polyphenol-Induced Adhesive Liquid Metal Inks for Substrate-Independent Direct Pen Writing

Md. Arifur Rahim,\* Franco Centurion, Jialuo Han, Roozbeh Abbasi, Mohannad Mayyas, Jing Sun, Michael J. Christoe, Dorna Esrafilzadeh, Francois-Marie Allieux, Mohammad B. Ghasemian, Jiong Yang, Jianbo Tang, Torben Daeneke, Srinivas Mettu, Jin Zhang, Md Hemayet Uddin, Rouhollah Jalili, and Kourosh Kalantar-Zadeh\*

Surface patterning of liquid metals (LMs) is a key processing step for LM-based functional systems. Current patterning methods are substrate specific and largely suffer from undesired imperfections—restricting their widespread applications. Inspired by the universal catechol adhesion chemistry observed in nature, LM inks stabilized by the assembly of a naturally abundant polyphenol, tannic acid, has been developed. The intrinsic adhesive properties of tannic acid containing multiple catechol/gallol groups, allow the inks to be applied to a variety of substrates ranging from flexible to rigid, metallic to plastics and flat to curved, even using a ballpoint pen. This method can be further extended from hand-written texts to complex conductive patterns using an automated setup. In addition, capacitive touch and hazardous heavy metal ion sensors have been patterned, leveraging from the synergistic combination of polyphenols and LMs. Overall, this strategy provides a unique platform to manipulate LMs from hand-written pattern to complex designs onto the substrate of choice, that has remained challenging to achieve otherwise.

## 1. Introduction

The unique blend of liquid properties and metallic conductivity has expanded the use of room temperature liquid metals (LMs) in diverse functional systems ranging from soft electronics and smart sensors to drug delivery and biotechnologies.<sup>[1–9]</sup> In many of these applications, along with the emerging ones, surface patterning of LMs is a key processing step. However, the development of efficient and accessible patterning methods of LMs onto different substrates is still challenging and requires a deeper understanding of the complex interfacial chemistry involved with LMs and their surroundings.<sup>[2,10–12]</sup>

Current strategies to pattern LMs onto substrates can be largely categorized as: 1) the use of LMs directly as inks for extrusion printing or writing,<sup>[13–16]</sup> and 2) the deposition of surface-stabilized LM dis-

persions (can be polymer or surfactant stabilized, or directly with native metal oxides) onto substrates where the mechanical sintering of the dispersed phase by an indenter or pressure bursting of the LM bubbles results in conductive traces in specific areas of the substrates.<sup>[17–22]</sup> These strategies are particularly suitable for microfluidic patterning or stencil writing with high metallic conductivity,<sup>[23]</sup> however while writing/patterning onto substrates, they suffer from limited interactions with the substrate surfaces of variable chemistries, limiting their universal application. On many substrates, the direct extrusion approach produces undesired pattern deformation, bulges, and flowing conductive traces due to the high surface tension ( $>400 \text{ mN m}^{-1}$ )<sup>[23,24]</sup> and incompatible fluidity of LMs. In addition, the oxide skin formation during the extrusion of LMs clogs the patterning nozzle.<sup>[13,23]</sup> On the other hand, the surface-stabilized LM dispersion strategy has shown specific disadvantages in relation to the dispersion stability, dispersion lifetime, and high spatial accuracy.<sup>[23,25,26]</sup>

Although the above challenges for a given system, can be mitigated to some extent with careful choice and intensive optimization of different components of the system, substrate specificity remains the common bottleneck in both the aforementioned printing/patterning strategies because of the limited

Dr. M. A. Rahim, F. Centurion, J. Han, R. Abbasi, Dr. M. Mayyas, J. Sun, M. J. Christoe, Dr. F.-M. Allieux, Dr. M. B. Ghasemian, Dr. J. Yang, Dr. J. Tang, Dr. R. Jalili, Prof. K. Kalantar-Zadeh  
School of Chemical Engineering  
University of New South Wales (UNSW)  
Sydney, New South Wales 2052, Australia  
E-mail: ma.rahim@unsw.edu.au; k.kalantar-zadeh@unsw.edu.au

Dr. D. Esrafilzadeh  
Graduate School of Biomedical Engineering  
University of New South Wales (UNSW)  
Sydney, New South Wales 2052, Australia

Dr. T. Daeneke, Dr. S. Mettu  
School of Engineering  
RMIT University  
Melbourne, Victoria 3001, Australia

Dr. J. Zhang  
School of Mechanical and Manufacturing Engineering  
University of New South Wales (UNSW)  
Sydney, New South Wales 2052, Australia

Dr. M. H. Uddin  
The Melbourne Centre for Nanofabrication  
Clayton, Victoria 3168, Australia

 The ORCID identification number(s) for the author(s) of this article can be found under <https://doi.org/10.1002/adfm.202007336>.

DOI: 10.1002/adfm.202007336

wettability stemming either from the high surface tension of LMs or inadequate adhesive interactions between the stabilized LM particles and substrate surface.<sup>[23,27]</sup> To overcome these challenges, a general approach to pattern LMs onto diverse substrates that is inexpensive and efficient, is highly sought after. In this context, the assembly of natural compounds on LM surfaces that can induce the desired properties such as adhesion and coordination to facilitate surface interactions (both with the LM particle and external substrate surfaces after assembly), can be a promising alternative.

In nature, various microorganisms use catechol-induced surface adhesion to survive in adverse environments.<sup>[28–32]</sup> Prominent examples include mussel byssus threads and sandcastle worm glue that are heavily functionalized with catechol groups.<sup>[33]</sup> Instances as such have inspired scientists to adopt biomimetic approaches using catechol-containing molecules to design coatings, adhesives, and functional materials that have found applications in various scientific disciplines.<sup>[29,34]</sup> In this

pursuit, plant polyphenols containing catechol/gallol groups have spurred significant attention in recent times, owing to their natural abundance and structural diversity.<sup>[29,35,36]</sup> In addition to their universal surface adhesion, polyphenols also exhibit a rich set of physicochemical properties such as metal coordination, self-assembly, redox, and stimuli responsiveness—making them an attractive class of functional building-blocks.<sup>[28,29]</sup>

Herein, we take inspiration from nature and integrate a naturally abundant polyphenol, tannic acid (TA, a multidentate ligand with multiple catechol/gallol functional groups ubiquitous in plant kingdom; its structure is shown in **Figure 1a**), with eutectic gallium-indium alloy (EGaIn) to prepare adhesive LM inks. We consider two important features for this particular combination: 1) similar to iron(III) ( $\text{Fe}^{3+}$ ) ions, the strong coordination interactions of  $\text{Ga}^{3+}$  ions with catechol functional groups (as established in the literature of iron–catechol chemistry),<sup>[36–38]</sup> may give rise to the coordination-driven assembly of TA on EGaIn particles and 2) the presence of multiple

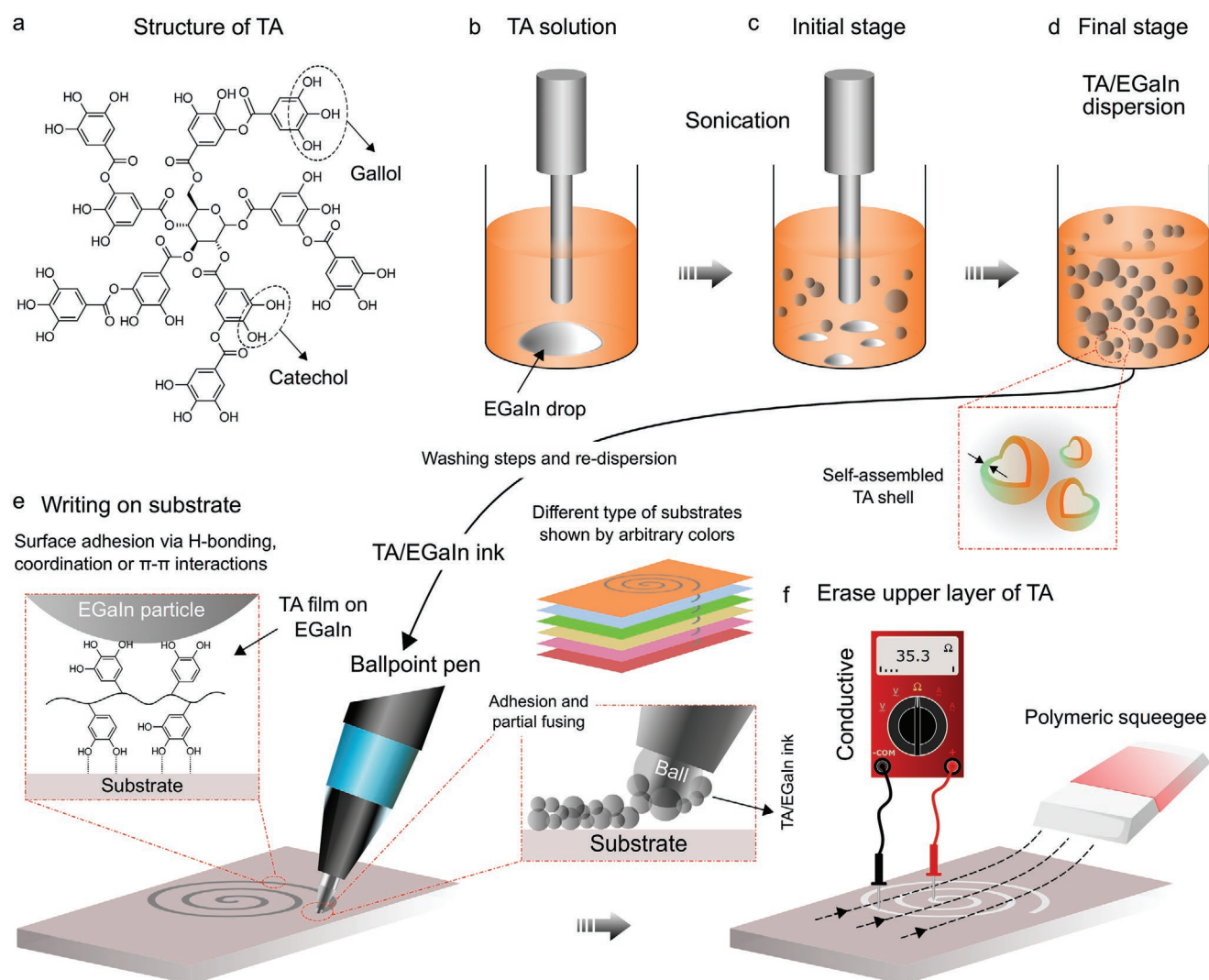


**Figure 1.** Schematic presentation of the ballpoint pen writing process. a) Structure of TA. b–d) Schematic of initial to final stages of the preparation of TA/EGaIn ink particles. e) Schematic of the writing/patterning process using a ballpoint pen filled with the TA/EGaIn inks. f) Transformation of the initial patterns to conductive by removing the phenolic layer using a soft polymeric squeegee.

catechol/gallol groups in TA may promote substrate surface adhesion after the assembly on EGaIn particles.<sup>[29,35,39,40]</sup> Using the TA/EGaIn inks, we demonstrate a ballpoint pen writing approach of LMs onto a variety of substrates (a total of 16 different substrates tested) enabled by the intrinsic adhesive nature of TA. The frictional force while writing, partially ruptures the assembled phenolic-shells of the LM particles—leading to particle fusion and conductive written traces after removal of the loosely adhered phenolic top layers. Complex conductive patterns could also be obtained on different substrates using an automated setup. This method of LM patterning enabled by an abundant natural compound with the desired adhesion for wide-ranging substrates should afford a general platform to fabricate smart electronic devices and advanced functional systems. As such, we sought to provide a few directions by demonstrating the patterned substrates as capacitive touch sensors and the ability of the ink particles to detect hazardous metal ions with enhanced sensitivity originating from the synergistic effect of TA and EGaIn.

## 2. Results and Discussion

The synthesis of TA/EGaIn ink and the subsequent ballpoint-pen writing process is schematically presented in Figure 1b–d. We adopted a top-down approach to prepare the TA/EGaIn ink. TA solution containing EGaIn drop was subjected to probe sonication for 30 min (see the Experimental Section for details), where the ultrasound stimulation disintegrated the large EGaIn droplets into nano- and micro-particles. Simultaneously, these particles were stabilized via the assembly of TA onto the EGaIn particle surfaces. After washing steps and redispersion, concentrated TA/EGaIn inks were obtained. A ballpoint-pen filled with the resulting inks was tested to write on a variety of substrates (as schematically shown in Figure 1e). The primary written traces were non-conductive due to the presence of the assembled TA layer (TA/EGaIn particles) and bulk TA molecules that could be removed by an ethanol washing step (for bulk TA) followed by gentle rubbing to fuse TA/EGaIn particles using a soft polymeric squeegee. This final process transformed the written traces conductive (Figure 1f and 3b for real samples).

We probed the chemical interactions occurring during the assembly process of TA on the EGaIn particles with a range of analytical techniques. Fourier transform infrared (FTIR) spectroscopic analyses of pure TA (Figure 2a) and TA/EGaIn particles revealed considerable differences. For example, the vibrational peaks characteristic of TA (black trace) such as, phenolic C–O stretching bands at 1532 and 1444  $\text{cm}^{-1}$ , and phenolic O–H bending vibrations at 1310 and 1174  $\text{cm}^{-1}$  were shifted to 1505, 1378  $\text{cm}^{-1}$ , and 1230, 1109  $\text{cm}^{-1}$ , respectively, in the TA/EGaIn particles (red trace). This indicates the possible coordination interactions involving  $\text{Ga}^{3+}/\text{In}^{3+}$  on the EGaIn particle surface and the gallol and/or catechol groups of TA. Additionally, the number of peaks detected in the TA/EGaIn particles was lower than that of TA, which is likely indicative of the formation of polymeric TA species on the surface of EGaIn particles (also see later for UV–Vis absorption). It should be noted that the polymerization of phenolic compounds such as natural polyphenols and dopamine, in an oxidizing environment is

well-established in literature.<sup>[28,29,41]</sup> Since the TA/EGaIn particles were prepared under sonication (i.e., an oxidizing environment), the polymerization and assembly of TA could occur simultaneously on the surface of EGaIn particles, where the assembly of TA species could be facilitated by the coordination interactions of the catechol/gallol groups of TA and  $\text{Ga}^{3+}/\text{In}^{3+}$ . Raman spectroscopy analysis of the TA/EGaIn particles (Raman spectra along with the relevant discussions are provided in Figure S1, Supporting Information) were also carried out, and the results correspond well with the FTIR results as above.

X-ray photoelectron spectroscopy (XPS) performed on the TA/EGaIn particles, revealed the presence of C 1s, O 1s, Ga 2p, and 3d, and In 3d peaks (Figure S2, Supporting Information) in the survey spectrum, which is consistent with the composition of the TA/EGaIn particles. Comparing the C 1s core-level spectra of pure TA with that of the TA/EGaIn particles (Figure 2b), the C–O peak at binding energy (BE) of 286.5 eV and C=O peak at BE 288.9 eV of TA were shifted to lower energy ( $\approx 0.2$  eV) in the latter. Additionally, the shake-up satellite peak at BE 291.7 eV (characteristic of aromatic carbon in TA) was not detected in the TA/EGaIn particles. These differences indicated that a complexed and/or modified form of TA is present in the TA/EGaIn particles (also see the discussion below). From the core-level Ga 3d XPS spectrum of TA/EGaIn particles (Figure 2c), the peak appeared at BE of 20.8 eV corresponds to  $\text{Ga}^{3+}$ , while the BE centered at 18.8 eV can be assigned to  $\text{Ga}^{1+}$ .<sup>[42]</sup> In contrast, the control EGaIn sample without TA exhibited the Ga 3d peaks at 20.1 ( $\text{Ga}^{3+}$ ) and 18.0 eV ( $\text{Ga}^0$ ).<sup>[42]</sup> Importantly, the peak for  $\text{Ga}^{3+}$  in the TA/EGaIn system was shifted to higher energy ( $\approx 0.8$  eV), indicating the coordination interactions of TA and  $\text{Ga}^{3+}$ , as it is known that the BE of a central atom increases with the increasing electronegativity of the attached atoms or groups.<sup>[43,44]</sup> Interestingly, In 4d peaks detected in the Ga 3d region were also different for the TA/EGaIn system when compared to EGaIn only. For example, we observed the doublet at  $\approx 16.0$  and  $\approx 16.8$  eV, which can be associated with the elemental In ( $\text{In}^0$ ) in the EGaIn sample, while the peaks at  $\approx 16.8$  and  $\approx 17.5$  eV detected for TA/EGaIn can be associated with  $\text{In}^{3+}$  ions. This aspect is further complemented by the analyses of the In 3d region for EGaIn and TA/EGaIn systems (spectra and relevant discussions are provided in Figure S3, Supporting Information). These results suggested that in addition to  $\text{Ga}^{3+}$  ions,  $\text{In}^{3+}$  ions were also involved in the coordination interactions with TA during the assembly process. As mentioned in the beginning, due to the presence of multiple catechol/gallol groups, TA is a potent ligand to coordinate strongly with a range of transition metals.<sup>[29,45]</sup> For example, iron–catechol chemistry has been extensively studied to understand mussel's adhesion and bacterial iron transport.<sup>[29,32,46]</sup> Owing to its similarity to  $\text{Fe}^{3+}$  ions (e.g., the ionic radii of  $\text{Fe}^{3+}$  and  $\text{Ga}^{3+}$  are 0.645 and 0.620 Å, respectively),<sup>[47,48]</sup>  $\text{Ga}^{3+}$  ions also exhibits strong coordination with catechol containing ligands. Additionally, the coordination interactions of catechol and  $\text{In}^{3+}$  ions are also well-documented.<sup>[44]</sup> The use of TA, therefore, both facilitates 1) the dispersion of LMs via strong surface coordination and subsequent assembly, and 2) the assembled TA films impart a set of functional properties to the composite LM particles (see applications later) including adhesiveness (Figure 1e) that promotes particle-surface interactions with external substrates.

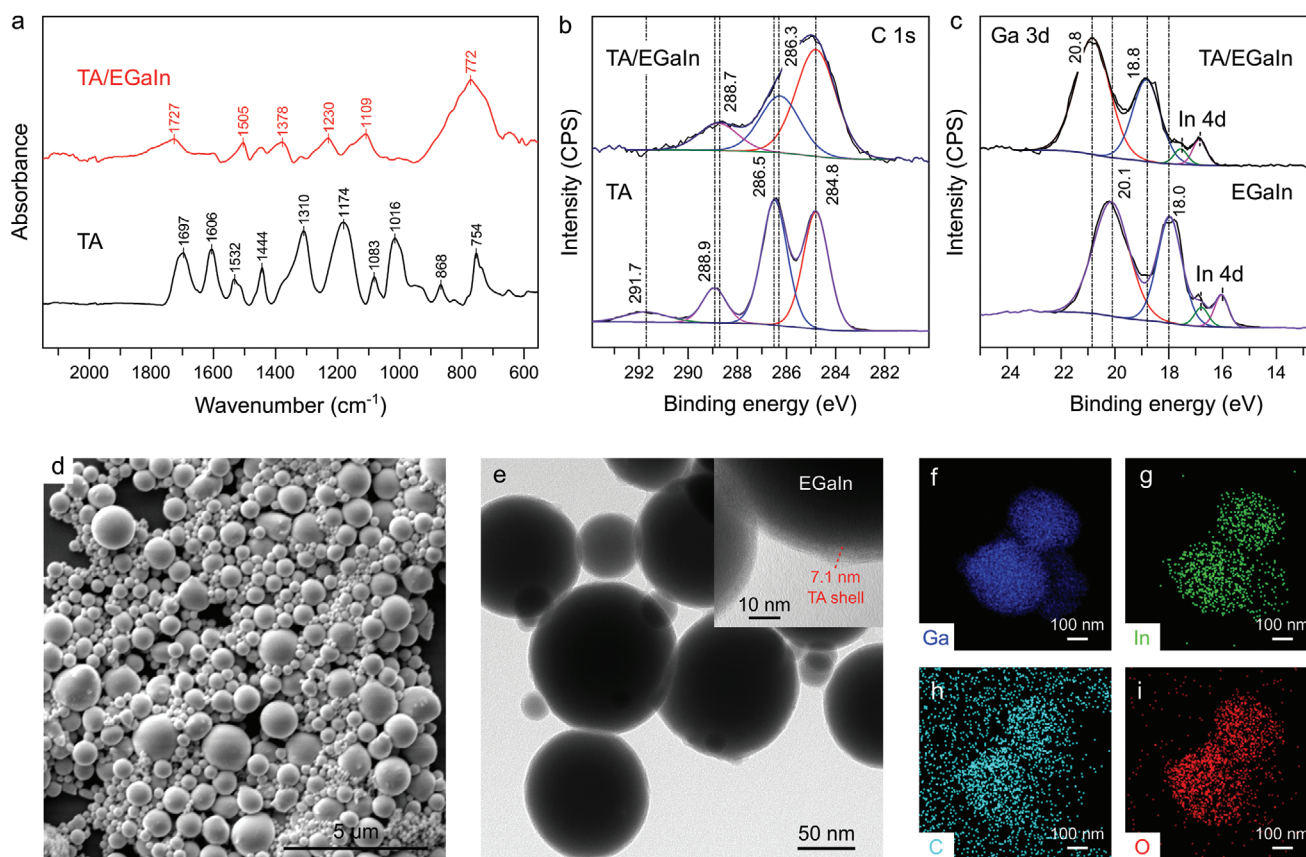


**Figure 2.** Characterization of TA/EGaIn ink particles. a) FTIR spectra of TA and TA/EGaIn particles. b) XPS C1s spectra of pure TA and TA/EGaIn particles. c) XPS Ga 3d spectra of EGaIn and TA/EGaIn particles. d) SEM micrographs showing the spherical shape of the TA/EGaIn particles. e) TEM images showing the self-assembled TA layer on the TA/EGaIn particles (inset). f–i) The corresponding EDS analyses of the TA/EGaIn particles.

Scanning electron microscopy (SEM) performed on the TA/EGaIn system indicated that the obtained particles were in spherical shape (Figures 2d) and polydisperse with the median size of  $\approx 360$  nm (Figure S4, Supporting Information). High resolution transmission electron microscopy (HRTEM) performed on the TA/EGaIn system also confirmed their spherical shapes and further confirmed the presence of an interfacial TA layer on the EGaIn particle surfaces. The thin organic layer observed had a thickness of  $\approx 7$  nm (Figure 2d,e). Since the size of TA is  $\approx 2$  nm,<sup>[36]</sup> this layer must have originated via crosslinking mechanisms involving covalent and/or coordination interactions. UV–Vis absorption spectroscopy performed on the supernatant obtained after desorbing (see the Experimental Section for details) the organic layer from the TA/EGaIn particles, also indicated the presence of polymeric species of TA (Figure S6, Supporting Information). These observations are consistent with our recent report on the dispersion of liquid Ga with gallic acid.<sup>[43]</sup> As shown in Figure 2f–i, energy-dispersive X-ray spectroscopy (EDS) mapping of the particles confirmed the composition of the TA/EGaIn inks as evident from the spatially concentrated signals of the Ga and In appearing from EGaIn and C and O appearing from TA. These results suggest that the assembly process of TA on EGaIn surface takes place via a complex mechanism of oxidative polymerization and coordination interactions involving both Ga and In ions. In addition, it is also possible

that during the sonication, some  $\text{Ga}^{3+}$  ions were released in the vicinity of the EGaIn particle surface and used by TA to extend the assembled layer thickness via coordination crosslinking. Furthermore, a small contribution to the layer thickness may have occurred by a concurrent process of self-polymerisation of TA<sup>[29,41]</sup> as observed by other spectroscopic investigations. A similar observation in relation to the release of  $\text{Ga}^{3+}$  ions and coordination by alginate to form an assembled alginate layer on EGaIn particle was also demonstrated previously.<sup>[49]</sup>

Next, the TA/EGaIn inks (Figure S5, Supporting Information) were employed to write LMs on various substrates with diverse surface chemistry and mechanical properties. We demonstrate a writing method with the inks using a ballpoint pen (Figure S7, Supporting Information). A regular ballpoint pen with a ball diameter of 0.7 mm was filled with the TA/EGaIn inks and used for writing on different substrates. While writing, the ballpoint pen moves across the substrate and the turning ball (wetted by the ink) forces the TA/EGaIn ink particles down the ink reservoir onto the ball. The ball in contact with the substrate then transfers the ink, and stable traces are formed due to the adhesive properties of the ink. The catechol and gallol functional groups in TA are known to promote surface adhesion via electrostatic, hydrogen bonding,  $\pi$ – $\pi$  stacking, and coordination interactions depending on the chemical nature of the substrate.<sup>[28,29,32]</sup> Due to this versatile adhesive

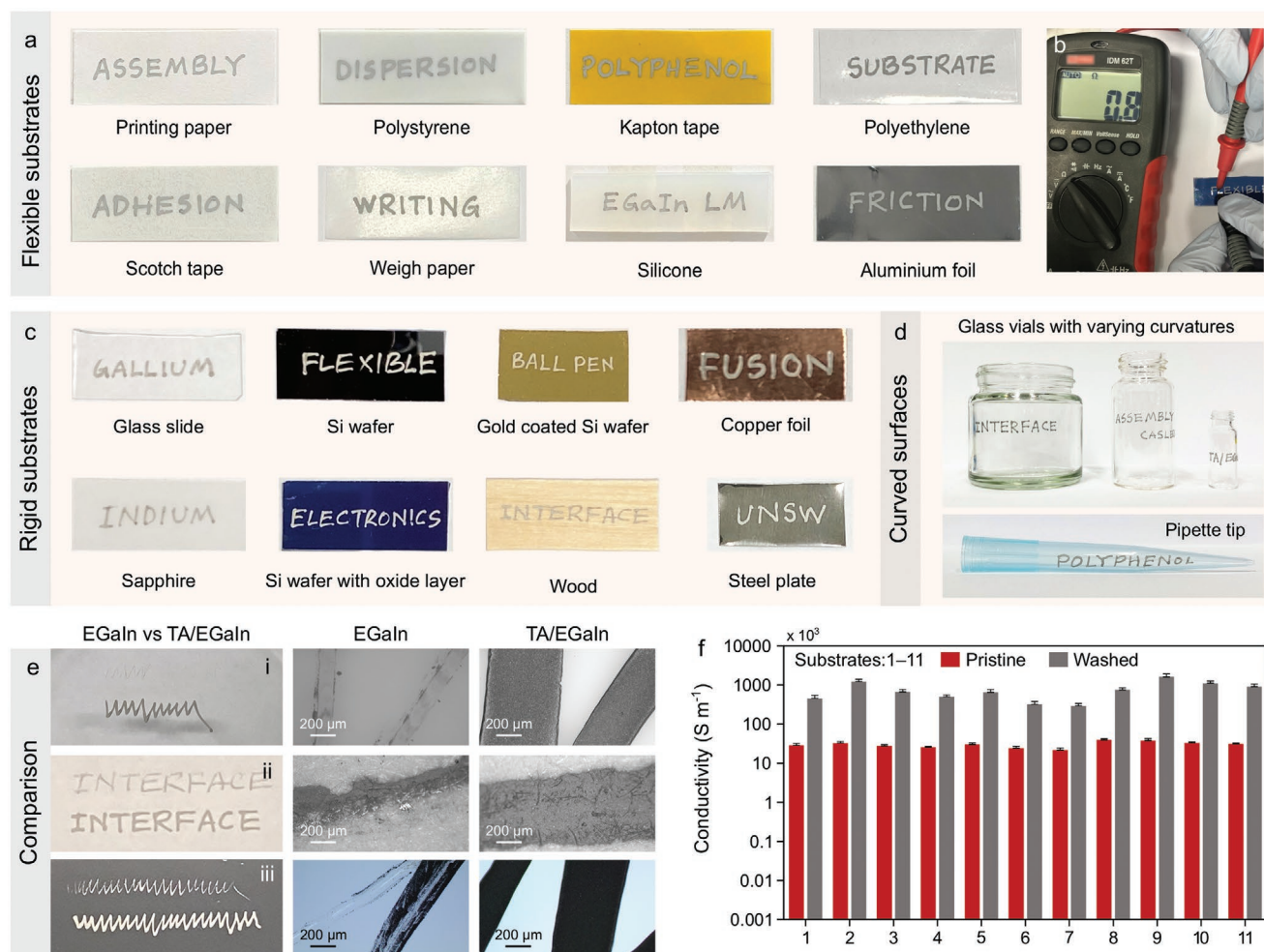


**Figure 3.** Hand-written traces by a ballpoint pen filled with the TA/EGaIn inks. a) Written traces on various flexible substrates. b) Resistance of the written conductive traces on printing paper after removal of the phenolic layer by a polymeric squeegee. c) Written traces on various rigid substrates. d) Written traces on various curved surfaces. e) Photographs (left column) showing the written (or attempted) texts and lines by EGaIn (top part in each substrate) and TA/EGaIn inks (bottom part in each substrate) on different substrates. Optical microscopy images (middle column for EGaIn inks and right column for TA/EGaIn inks) of the corresponding sections of the written texts and lines. f) Conductivity of the written traces on different substrates after removal of the phenolic layer by a polymeric squeegee: 1, printing paper; 2, polystyrene; 3, Kapton tape; 4, polyethylene; 5, Scotch tape; 6, weigh paper; 7, silicone; 8, glass; 9, Si wafer; 10, Si wafer with oxide layer; 11, Sapphire.

nature of TA, writing with the TA/EGaIn ink was possible on diverse substrates. Smooth written texts were obtained on 16 different substrates (as shown in **Figure 3a,c**, each substrate size was  $\approx 2 \text{ cm} \times 5 \text{ cm}$ ) that ranged from polymeric to metal and metal oxide surfaces with mechanical properties of the substrates ranging from rigid to flexible. On these substrates, we wrote several keywords associated with this study. The ink viscosity was optimized ( $\approx 22 \text{ mPa}\cdot\text{s}$ ) to write as easily as regular writing inks. After fusing the particles by a soft polymeric squeegee (with and without an intermediate washing step to remove bulk TA), the written traces could be turned conductive as shown on Si (**Figure 3b**; **Figure S8**, Supporting Information) substrates. This approach is also applicable to curved surfaces made of different materials as shown in **Figure 3d**, where the texts were smoothly written on glass vials with varying diameter and a pipette tip (polypropylene). In sharp contrast, when the ballpoint pen was filled with an ink of EGaIn without TA

(control, see the Experimental Section for details), writing was incoherent and patchy (even in cases, was not possible) regardless of the substrate type as it quickly clogged the pen nib as shown in **Figure 3e** (i–iii). This ink also showed limited flowability and surface interactions with the tested substrates. To compare, examples of written traces of EGaIn and TA/EGaIn inks on polystyrene, writing paper, and Si wafer are presented in **Figure 3e**. Photographs (left column) showing the written (or attempted) texts and lines by EGaIn (top part in each substrate) and TA/EGaIn inks (bottom part in each substrate) on different substrates. Optical microscopy images (middle column for EGaIn inks and right column for TA/EGaIn inks) of the corresponding sections of the written texts and lines are also presented indicating the difference in writing quality of the systems. Attempt to write with a surfactant/LM ink also mostly failed as shown in **Figure S9**, Supporting Information. The width of the written traces on different substrates was found

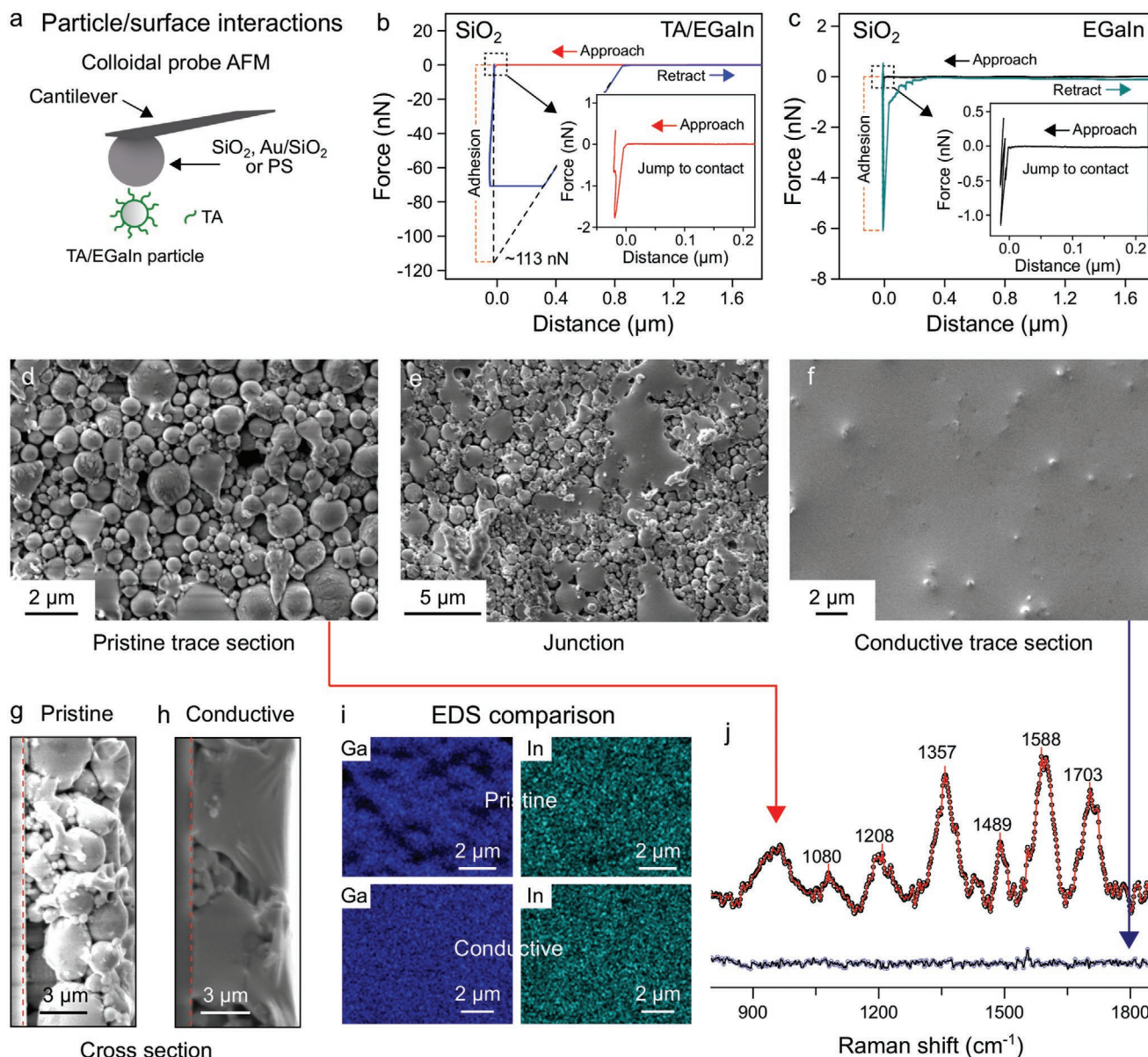


**Figure 4.** Substrate–particle adhesion and characterization of different writing stages. a) Schematic showing the substrate–particle interaction measured using a colloidal probe in force spectroscopy (AFM). b) Force curves showing the adhesion between a TA/EGaIn particle and colloidal SiO<sub>2</sub> probe; inset presents the approach curve at high magnification. c) Force curves showing the adhesion between an EGaIn particle and colloidal SiO<sub>2</sub> probe; inset illustrates the approach curve at high magnification. d–f) SEM micrographs of the different sections of the written trace after squeegee rubbing pristine, junction, and conductive sections, respectively. g,h) Cross-sectional SEM micrographs of the pristine and conductive sections of a written trace. i,j) The corresponding EDS and Raman analyses of the pristine and conductive sections of a written trace.

to be in the range of 500 to 600 μm, while the thickness varied from 6 to 8 μm (as an example, a cross-sectional SEM micrograph of a written trace on Si wafer, is provided in **Figure 4**).

The conductivity values of the written traces after applying the squeegee calculated from the observed resistance were in the range of  $2.1 \times 10^4$  to  $3.9 \times 10^4$  S m<sup>-1</sup> (Figure 3f). However, when the traces after writing and drying were washed in ethanol to remove the residual TA present in the ink (not the assembled TA layer), the conductivity of the written traces could be significantly improved with values in the range of  $2.9 \times 10^5$  to  $1.6 \times 10^6$  S m<sup>-1</sup> for different substrates (note that the metallic

substrates such as steel, copper, aluminium, and gold coated Si wafer, have been omitted from this calculation as being inherently conductive). These values are higher than many LM and non-LM based conductive patterns and comparable to some of the best in the field.<sup>[22,23]</sup> For example, Guo et al. reported a printing process based on magnetic EGaIn particles with a conductivity of  $1.53 \times 10^6$  S m<sup>-1</sup>.<sup>[50]</sup> Liu et al. used a laser sintering for spray printed EGaIn particles with conductivity values in the range of  $3 \times 10^5$  to  $3.625 \times 10^6$  S m<sup>-1</sup>.<sup>[51]</sup> Li et al. by using cellulose nanofiber and alginate based LM printing processes, reported conductivity values of  $8.9 \times 10^5$  S m<sup>-1</sup> (evaporation

induced sintering) and  $\approx 4.8 \times 10^5 \text{ S m}^{-1}$  (mechanically sintered), respectively.<sup>[49,52]</sup> However, these reported printing processes are complex and substrate specific as mentioned in the introduction. The variation of conductivity of the written traces using TA/EGaIn ink was found to be negligible after a trace on paper substrate was treated at 50 °C for 24 h (Figure S10, Supporting Information). Furthermore, the LMs can be recovered from the written traces as shown in Figure S11, Supporting Information.

Considering that the adherence of the TA/EGaIn ink particles deposited on the surface, while writing, is governed by the interactions between the assembled TA layer and substrate surface, the adhesion properties of the TA/EGaIn ink particles onto different substrates were examined by AFM colloidal probe force spectroscopy.<sup>[35]</sup> The colloidal probe (an example is provided in Figure S12, Supporting Information), acting as the substrate, was brought to contact individual ink particles and the probe/particle (i.e., substrate/particle in this case as shown in Figure 4a) interactions were monitored. The adhesion force ( $F_{\text{ad}}$ ) can be determined from the cantilever retraction cycle. As presented in Figure 4b,c), a large adhesive force was observed for the TA/EGaIn particle when compared to an EGaIn particle, that is, 113 nN versus 6 nN. During the probe approach, the difference in long-range interactions was also observed considering the forces associated with the jump-in-contact points for TA/EGaIn and EGaIn particles, as shown for both the systems in Figure 4b,c (inset). Similarly, the adhesive forces for TA/EGaIn particles measured by gold-coated silica (i.e., gold substrate) and polystyrene colloidal probes were also found to be remarkably higher than that of EGaIn particles as shown in Figures S13 and S14, Supporting Information. These results were further corroborated by bulk adhesion measurements performed by peel-off and tape tests, where using different substrates (an example with aluminium substrate is shown in Figure S15, Supporting Information) the adhesion difference could be observed comparing the TA/EGaIn and EGaIn ink systems.

To demonstrate the squeegee rubbing process to make the traces conductive, SEM images (Figure 4d–f) of a partially fused line is demonstrated where the junction shows both fused and deposited particle section where the left and right of the junction present the pristine and fused particles, respectively. The applied pressure from the squeegee breaks the TA shells of the ink particles and the EGaIn droplets start to flow and fuse together. Cross-sectional SEM images of the traces (Figure 4g,h) show that the fusion occurred in the bulk as well. The corresponding Raman and SEM analyses are also presented for clarity (Figure 4i,j). While in the Raman analyses, the presence and absence of TA layer (the associated peaks are discussed in Figure S1, Supporting Information) was obvious, EDS analyses show the morphological difference in the trace sections of pristine and fused particles. The width of the line trace can be correlated with the effective ball diameter during writing suggesting that  $\approx 90\%$  of the rolling ball surface was active during writing. When the pen nib after writing was probed under SEM, we observed that the outer part of the ball was covered with the ink particles (Figure S16, Supporting Information) while the center part in contact with the surface showed some particle fusion due to the friction while writing.

The handwriting method described above, could also be translated to fabricate complex patterns. We used a 3D printer and replaced the printing nozzle with a ballpoint pen filled with the TA/EGaIn inks. The printer was programmed in such a way that the patterns were produced via a single layer writing (see Figure 5a). We provide several examples of the patterns on different substrates (Figure 5b–d) such as spiral patterns on paper or Si wafer, a spider web on plastic (polypropylene), and a Voronoi pattern on paper substrates. Note that the spider web pattern appears to be thicker because of the trace overlapping (i.e., double layer printing) as the printer moved the pen on existing written trace before moving to write a new section. These patterns were turned to conductive either by the rubbing method (by applying a polymeric squeegee) or a roller pressing method described elsewhere.<sup>[43]</sup> Using the roller pressing method the conductivity values of the patterns on flexible substrates (Figure S17, Supporting Information) were found to be higher than the squeegee method and were in the range of  $1.0 \times 10^6$  to  $1.2 \times 10^6 \text{ S m}^{-1}$ . This is possibly because of the better fusion of the particles under controlled mechanical pressure (Figure S18, Supporting Information). The resulting conductive patterns decorated with light emitting diodes (LEDs) were then tested applying a voltage across the pattern that successfully turned on the LEDs as shown in Figure 5e.

Development of soft and flexible electronics is critically important for next-generation electronic devices. In this context, LM based systems have made considerable promise in recent times.<sup>[2,53,54]</sup> However, due to their unfavorable surface interactions, the compatible range of substrates is generally limited at present. In contrast, our adhesive LM inks can be written on diverse types of substrates that holds promise to expand the realm of applications of LMs in soft and flexible electronics. We demonstrate some typical features of using flexible substrates with the conductive written traces. As demonstrated by the photographs in Figure 5f,g, the components of the setup could be kept in proper functional status where the LEDs could be turned on normally under different deformations of the substrates such as bending and folding. Different substrates such as writing paper and Kapton tape are shown as representative examples. Bending experiments in multiple cycles with Kapton (5 cm long trace with an initial end to end resistance of 15.2  $\Omega$ ) at two different radii of curvature resulted in minor change of resistance within 0.1% over 500 cycles as shown in Figure 5h. Similarly, folding experiments with paper (3 cm long trace with an initial end-to-end resistance of 12.9  $\Omega$ ) substrate at two different angles showed negligible changes in resistance over 500 cycles. In addition, we also fabricated a stretchable conductive trace using nitrile substrate as shown in Figure 5j, where an LED could be kept functional under different strains. In Figure 5k, the change in resistance due to deformation of the trace, under various strains up to 70%, follows a semi linear increase in resistance as a function of the applied strain. The mechanical durability of the written trace was also evaluated by a repeated strain test (50% strain) in over 500 cycles (Figure 5l) and the change in resistance was observed to be negligible.

The efficient direct-writing method of the adhesive LM ink enabled by TA should attract a range of applications across different disciplines. We aim to provide a couple of directions here. First, we demonstrate the use of TA/EGaIn conductive pattern

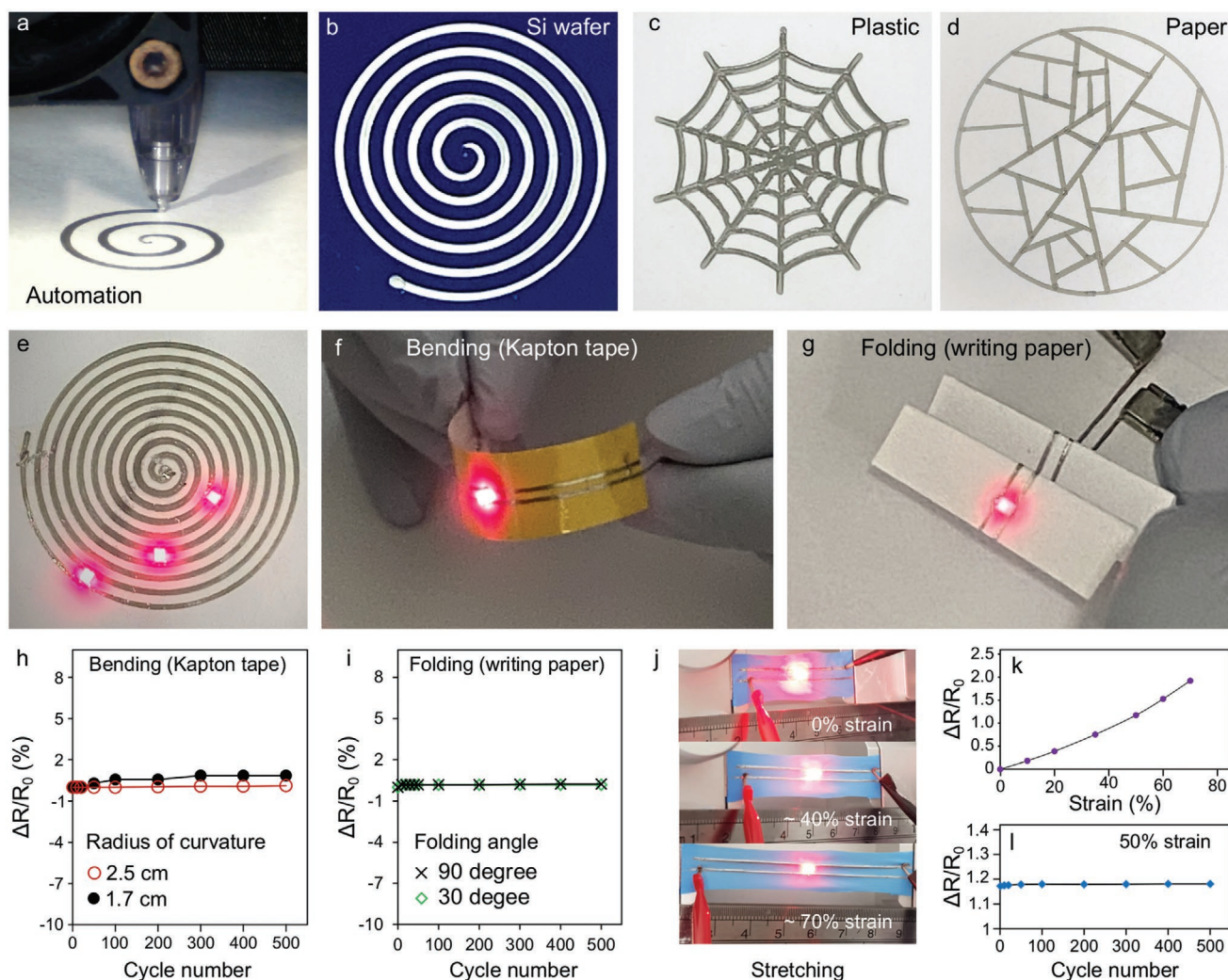


**Figure 5.** Complex patterns fabricated using an automated set-up. a) Photograph of the TA/EGaIn ink filled ballpoint pen, while patterning. b–d) Photographs of spiral, spider-web, and Voronoi patterns on Si wafer, plastic, and writing paper substrates, respectively. e) Photograph of spiral pattern on writing paper decorated with LEDs after lighting up. Photographs of hand-written lines (with the aid of a ruler) after fusing the particles, showing the conductivity upon bending (f) and folding (g). Resistance change over multiple cycles for bending (h) and folding (i) tests. j) Example of conductive stretchable substrate decorated with an LED at different strains. Resistance change of the stretchable substrate at different strains (k) and over multiple cycles at 50% strain (l).

written on different substrates for capacitive touch sensing. **Figure 6a** presents the diagram of the equivalent circuit of the sensor design. A photograph of the conductive spiral pattern used as the touch sensor is shown in Figure 5b. When the sensor was touched by a fingertip (Figure 6b), the capacitive response changed. The real time variation in capacitance with multiple touches is shown in Figure 6c. A total of 11 consecutive touches (each touch lasted about 3 s with an interval of  $\approx 2$  s between touches) followed by a longer touch (7 s) resulted in similar changes in the capacitive response, where the response (rise time,  $\tau$ ) changed from  $\approx 100$  to  $\approx 125$   $\mu$ s. The sensor response was found to be quite stable with each touch and could be repeated over a long period time (monitored over a week) without losing its typical response behavior. Additionally, a hand-written pattern on Kapton tape used as a touch sensor displayed similar responsive behavior as shown in Figure S19, Supporting Information.

LMs are known to amalgamate a range of different heavy metals—an intriguing property suitable for toxic metal sensing.<sup>[55]</sup> Earlier we demonstrated the sensing ability of LM particles for heavy metal ions using Galinstan (an alloy of Ga, In, and Tin) and its composites.<sup>[56,57]</sup> Incorporation of metal oxide (e.g., tungsten oxide) nanoparticles on the surface of Galinstan particles was observed to enhance the detection sensitivity of the heavy metal ions that was attributed to 1) the generation of a localized electric field at the nanoparticle/LM/electrolyte triple phase boundary and 2) the surface area produced by the nanoparticles with a high surface to volume ratio.<sup>[56]</sup> In contrary to the previous reports of embedding inorganic nanoparticles on LM surface, we hypothesized that the TA/EGaIn particle system with the TA nanofilm on the EGaIn particles could serve as an integrated system for toxic metal detection, where the coordination ability of TA could result

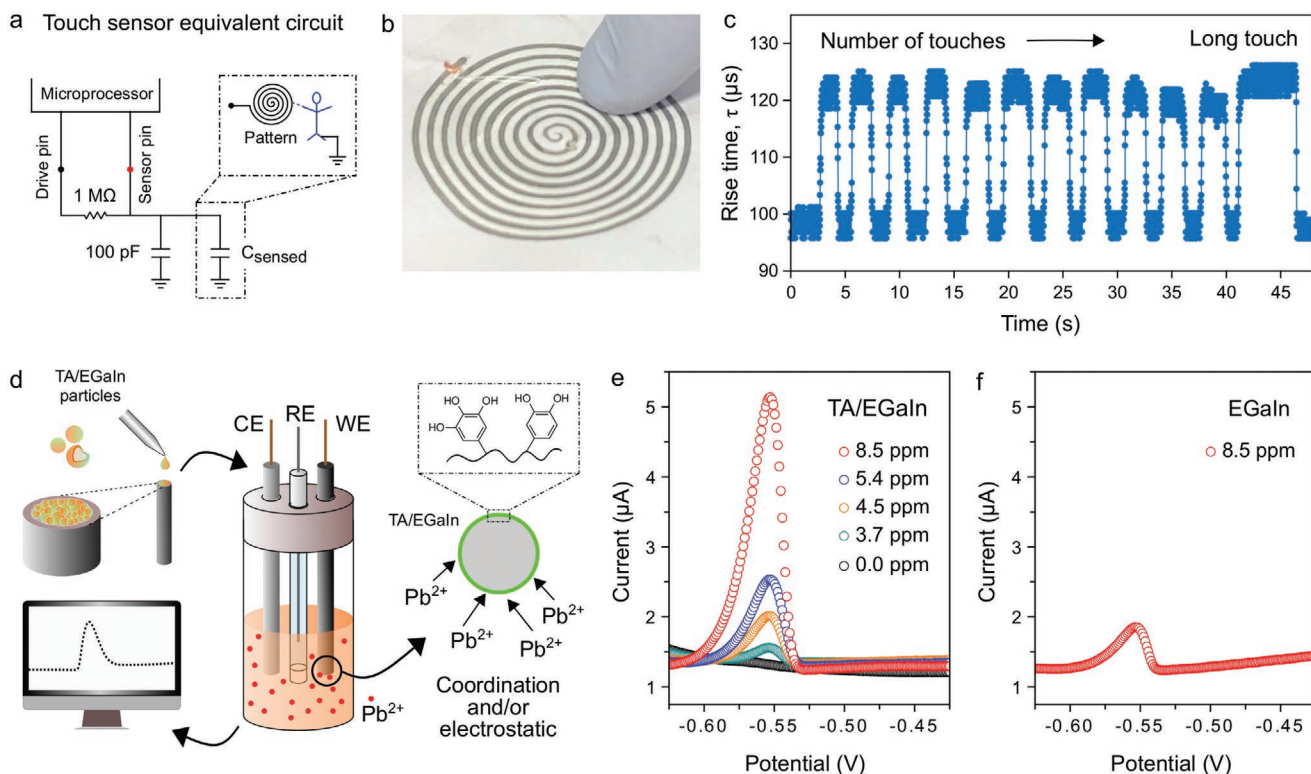


**Figure 6.** Applications of TA/EGaIn ink system. a–c) Touch sensor based on the conductive pattern prepared from TA/EGaIn ink system; equivalent circuit diagram, photograph of the spiral conductive pattern (on paper) used for touch sensing and the capacitive change of the sensor with consecutive number of touches, respectively. d) Schematic showing electrochemical assembly for  $\text{Pb}^{\text{II}}$  ion sensing by the TA/EGaIn particles. e) Electrochemical  $\text{Pb}^{\text{II}}$  ion sensing with increasing concentration by the TA/EGaIn particles. f)  $\text{Pb}^{\text{II}}$  ion sensing by control EGaIn (without TA) particles for comparison.

in enhanced detection sensitivity of the system. To test this hypothesis, we investigated the potential of TA/EGaIn particles for lead ion ( $\text{Pb}^{2+}$ ) sensing. The electrochemical setup used in this case is schematically shown in Figure 6d. The experiments were performed using a glassy carbon electrode (working electrode, WE) modified with TA/EGaIn ink particles. Differential pulse anodic stripping voltammetry was carried out as a function of  $\text{Pb}^{2+}$  concentration in a buffer solution of pH 4.5. The differential pulse voltammograms were recorded over the potential range of  $-0.65$  to  $-0.15$  V. The oxidation peak potential for Pb was detected at  $-0.55$  V that agrees well with the previous reports.<sup>[56,57]</sup> The intensity of this oxidation peak increased with the increasing concentration of  $\text{Pb}^{2+}$  ion (Figure 6e). The TA/EGaIn system showed a current amplitude of  $\approx 5 \mu\text{A}$  at  $\text{Pb}^{2+}$  concentration of 8.5 ppm. In contrast, control EGaIn particles without TA showed a current amplitude of  $\approx 2 \mu\text{A}$  in identical conditions (Figure 6f). These results indicate the synergistic impact of TA and EGaIn particles for  $\text{Pb}^{2+}$  sensing that possibly arise from the coordination ability of TA that facilitates the accumulation and diffusion of  $\text{Pb}^{2+}$  ions onto the electrode. The  $\text{Pb}^{2+}$  ions coordinated to TA on the EGaIn particles, could be easily reduced to elemental Pb, thereby increasing the sensitivity of the system. This process is schematically presented in Figure S20, Supporting Information. Similar role of TA for a TA-modified gold nanoparticle system for mercury ion ( $\text{Hg}^{2+}$ ) detection was also observed previously.<sup>[58,59]</sup>

### 3. Conclusion

Here we presented a biomimetic approach to pattern LMs onto diverse substrates. This was inspired by the universal catechol adhesion exhibited by various microorganisms. Using a ubiquitous plant polyphenol, tannic acid, which is comprised of multiple catechol/gallol functional moieties, we demonstrated the preparation of a new class of adhesive LM inks and their utilization for writing and patterning of LMs in a substrate-independent manner. This is an important feature that had remained difficult to achieve with the current LM patterning methods such as direct extrusion and surface-stabilized LM dispersions with native oxide skins or synthetic surfactants/polymers, lacking the desired adhesion properties for substrates displaying diverse chemistries. We anticipate that the method described here, that is, the use of a natural compound with properties perfectly suitable for LM dispersion and subsequent patterning on diverse substrates, will lead to new avenues for a range of applications. To support this claim, we presented a few directions here. First, we demonstrated the application of the patterned substrates as capacitive touch sensors. Second, we provided a proof-of-concept using the ink particles for hazardous heavy metal ion sensing with improved sensitivity by taking advantage of the synergy of LMs and polyphenols. Overall, the presented approach offers a unique platform to pattern LMs in a substrate-independent manner, and also provides fundamental insights into the interfacial chemistry of LM nanoparticles.

## 4. Experimental Section

**Materials:** Gallium (Ga, beads, 99%) and indium (In, beads, 99.9% purity) were purchased from Roto metals, USA. TA, lead sulfate, acetic acid, ammonium acetate, and ethanol were purchased from Sigma-Aldrich and used as received. High-purity (Milli-Q) H<sub>2</sub>O with a resistivity of 18.2 M $\Omega$ -cm was obtained from an inline Millipore RiOs/Origin H<sub>2</sub>O purification system.

**Synthesis of TA/EGaIn Inks:** Eutectic gallium-indium (EGaIn) alloy was obtained by melting 74.5 wt% Ga and 25.5 wt% In at 80 °C for 30 min with occasional stirring with a glass rod. In a typical synthesis of the TA/EGaIn ink, 1 mL of EGaIn was added to a glass vial containing ethanolic solution of TA solution (20 mL, 25 wt%, i.e., 250 mg mL<sup>-1</sup>). The mixture was then sonicated at 30% power for 30 min using a probe sonicator (VCX 750, Sonics & Materials, Inc.). After sonication the vial was taken out and the dispersion was washed with ethanol twice via centrifugation (4700 rcf) to discard the excess reactants. The obtained particles were finally re-dispersed in 1.5 mL of TA solution (25 wt% in ethanol) and vortexed to obtain the ink solution. The TA/EGaIn ink remains stable and useable if stored in a sealed container to avoid ethanol evaporation. However, large particles in the inks tend to settle down after a long-term storage, so shaking or vortexing before use is required. Particle size can be altered by increasing the sonication time as shown in Figure S4, Supporting Information.

Samples for TEM, SEM, FTIR, and Raman spectroscopy assessments were prepared using the sonicated samples after the ethanol washing steps and re-dispersion in ethanol. Samples were drop-casted on Si wafer (SEM, FTIR, and Raman) or Cu grid (TEM). The organic layer formed on the TA/EGaIn particles was also investigated by UV-Vis absorption spectroscopy. Briefly, the TA/EGaIn particle sample obtained after the ethanol washing steps (as above) was washed twice with water by centrifugation and then incubated in 10 mL of 0.1 M HCl to desorb the organic layer from the particle surfaces. The resulting suspension was centrifuged, and the supernatant was collected for UV-Vis absorption measurements.

The control EGaIn ink without TA was prepared in an identical manner as above. Briefly, 1 mL of EGaIn was added to a glass vial containing 20 mL of ethanol. The mixture was then sonicated at 30% power for 30 min using a probe sonicator (VCX 750, Sonics & Materials, Inc.). After sonication the vial was taken out and the dispersion was washed with ethanol twice via centrifugation (4700 rcf). The obtained particles were finally re-dispersed in 1.5 mL of ethanol and vortexed to obtain the control ink solution. A surfactant/EGaIn ink was also prepared using Tween 20 (30% v/v, in ethanol) in identical manner as above and tested for ballpoint pen writing.

**Handwriting with a Ballpoint Pen:** A regular ballpoint pen (Pilot, ball diameter of 0.7 mm) was first washed thoroughly to remove the originally present writing inks. The washed tube of the pen was then filled with the TA/EGaIn ink (300  $\mu$ L) and the pen was ready to use. Writing and patterning was performed on a range of substrates including printing paper, weigh paper, polystyrene, Kapton tape, polyethylene, Scotch tape, silicone, glass, Si wafer, Si wafer with oxide layer, aluminium foil, gold coated Si wafer, copper, steel plate, and sapphire disk. The substrates were cut into  $\approx$  2 cm  $\times$  5 cm (width  $\times$  length) size. Writing tests were also performed with the control EGaIn ink in an identical manner.

**Transformation of the Written Traces to Conductive:** A soft polymeric squeegee was employed to transform the pristine written traces to conductive via particle fusing. A nominal pressure of 0.25 N was used to press the sample with the squeegee (2 cm width and 2 mm thickness) and moved along the traces. For higher conductivity, before applying the squeegee, the trace containing substrates were washed by gently dipping the substrates in ethanol and dried in air. This step removed the bulk TA present in the ink traces. Note that due to the manual nature of the rubbing process, a thickness loss of  $\approx$ 10% was observed. The conductor volume for 1 cm long trace varied from  $2.3 \times 10^{-5}$  to  $3.8 \times 10^{-5}$  cm<sup>3</sup> (estimated from the observed thickness and width of the traces by optical microscopy), depending on the substrate. For complex patterns (see below) on flexible substrates, the pristine patterns were washed

in ethanol and passed through a mechanical roller pressing device as described previously.<sup>[43]</sup>

**Automated Complex Patterning with a Ballpoint Pen:** A ballpoint pen identical to the one used for handwriting, was used in this case. The pen was set in place of the nozzle of a programmable 3D printer (LulzBot Mini) with a customized bouncing part which has the function of self-adjusting height. To ensure the continuous flow of the ink, the variables, that is, the pressure between the ballpoint pen and substrate, and the printing speed were optimized. The bouncing mechanical part of the printer regulates the pressure applied from the ballpoint pen to the substrate by self-adjusting the height while printing. After several preliminary tests, the suitable printing speed was found to be 2.5 mm s<sup>-1</sup>. The designs to be printed were pre-installed in the computer of the printer. Inkscape software (version 0.92.4) was used to design the vector pattern and generate the printing path file directly in G code. Different substrates such as writing paper, plastics, and Si wafer were used for patterning the TA/EGaIn inks.

**Touch Sensor:** A regular writing paper with a spiral pattern (obtained using the 3D printer) and a Kapton tape substrate with a hand-written pattern were used as the touch sensing platforms, where an integrated electronic device attached to each set up measured the capacitance change with touches (by a fingertip). The sensor element was connected in an RC circuit to an Arduino Uno development board in order to drive the sensor circuit with a step-function voltage signal and measure its rise time response.

**Hazardous Heavy Metal Ion Sensing:** The working electrode (WE) for lead ions (Pb<sup>2+</sup>) detection was prepared by drop casting 3  $\mu$ L of TA/EGaIn particle dispersion (identical to the dispersion prepared for SEM, FTIR, and Raman spectroscopy as described in the section of "Synthesis of TA/EGaIn Ink") on a glassy carbon electrode (diameter of 3 mm). WE modified with EGaIn particle dispersion (control, without TA) was prepared in identical manner as above. All measurements were performed using an Autolab Potentiostat (Autolab M204) electrochemical analyzer. The reference electrode (RE) was Ag/AgCl (sat. KCl) and platinum wire with fritted glass was used as the counter electrode. A basing three-electrode configuration was used for the electrochemical measurements. The electrochemical measurements were commenced after bubbling the electrolyte solutions with nitrogen gas for at least 10 min prior to any measurement. For stripping voltammetry, 0.1 M acetate buffer solutions with a pH of 4.5 were used as the supporting electrolyte, which was prepared from ammonium acetate and acetic acid (99.7%) in Milli-Q water. Lead ions (Pb<sup>2+</sup>) were incorporated in the supporting electrolyte by dissolving lead (II) sulfate. Prior to every scan, a preconditioning step (60 s at -0.65 V versus Ag/AgCl) was carried out. The voltammogram was recorded by applying a positive-going scan from -0.65 to -0.15 V versus Ag/AgCl (step increment: 5 mV, amplitude: 80 mV, and pulse period: 0.2 s).

## Supporting Information

Supporting Information is available from the Wiley Online Library or from the author.

## Acknowledgements

The authors would like to acknowledge the Australian Research Council (ARC) Laureate Fellowship Grant (FL180100053) for the financial coverage of this study. This work was also performed in part at the Melbourne Centre for Nanofabrication (MCN) in the Victorian Node of the Australian National Fabrication Facility (ANFF). The authors also thank the technical assistance from The Aeronautical, Mechanical, and Mechatronics Engineering Laboratories (AMMELabs) at the University of Sydney.

## Conflict of Interest

The authors declare no conflict of interest.

## Author Contributions

M.A.R. and K.K.-Z. perceived the idea and designed the experiments. M.A.R. conducted the experiments and carried out the characterizations with the help of F.C., J.H., R.A., M.M., J.S., M.J.C., D.E., F.A., M.B.G., J.Y., J.T., and R.J. S.M. performed the AFM force measurements. J.Z. performed the T-peel tests. The following authors contributed to the data analyses, scientific discussions, and preparation of the manuscript: M.A.R., F.C., J.T., S.M., M.M., M.J.C., J.Z., M.H.U., T.D., and K.K.-Z. All authors revised the manuscript and provided useful comments.

## Keywords

assembly, direct writing, inks, liquid metals, natural polyphenols, universal adhesion

Received: August 28, 2020

Revised: November 3, 2020

Published online: December 11, 2020

- [1] T. Daeneke, K. Khoshmanesh, N. Mahmood, I. A. de Castro, D. Esrafilzadeh, S. J. Barrow, M. D. Dickey, K. Kalantar-zadeh, *Chem. Soc. Rev.* **2018**, *47*, 4073.
- [2] K. Kalantar-Zadeh, J. Tang, T. Daeneke, A. P. O'Mullane, L. A. Stewart, J. Liu, C. Majidi, R. S. Ruoff, P. S. Weiss, M. D. Dickey, *ACS Nano* **2019**, *13*, 7388.
- [3] F. Li, J. Shu, L. Zhang, N. Yang, J. Xie, X. Li, L. Cheng, S. Kuang, S.-Y. Tang, S. Zhang, W. Li, L. Sun, D. Sun, *Appl. Mater. Today* **2020**, *19*, 100597.
- [4] S. A. Chechetka, Y. Yu, X. Zhen, M. Pramanik, K. Pu, E. Miyako, *Nat. Commun.* **2017**, *8*, 15432.
- [5] L. Fan, M. Duan, Z. Xie, K. Pan, X. Wang, X. Sun, Q. Wang, W. Rao, J. Liu, *Small* **2020**, *16*, 1903421.
- [6] Y. Yu, E. Miyako, *iScience* **2018**, *3*, 134.
- [7] Y. Zhang, J. Sun, Q. Wang, S. Chen, L. Yao, W. Rao, J. Cai, W. Wu, *AIP Adv.* **2020**, *10*, 015226.
- [8] Y. Yu, E. Miyako, *Chem. - Eur. J.* **2018**, *24*, 9456.
- [9] H. Wang, Y. Yao, Z. He, W. Rao, L. Hu, S. Chen, J. Lin, J. Gao, P. Zhang, X. Sun, X. Wang, Y. Cui, Q. Wang, S. Dong, G. Chen, J. Liu, *Adv. Mater.* **2019**, *31*, 1901337.
- [10] L. Tang, S. Cheng, L. Zhang, H. Mi, L. Mou, S. Yang, Z. Huang, X. Shi, X. Jiang, *iScience* **2018**, *4*, 302.
- [11] N. Kazem, T. Hellebrekers, C. Majidi, *Adv. Mater.* **2017**, *29*, 1605985.
- [12] S.-Y. Tang, R. Qiao, S. Yan, D. Yuan, Q. Zhao, G. Yun, T. P. Davis, W. Li, *Small* **2018**, *14*, 1800118.
- [13] J. W. Boley, E. L. White, G. T. C. Chiu, R. K. Kramer, *Adv. Funct. Mater.* **2014**, *24*, 3501.
- [14] H. Chang, P. Zhang, R. Guo, Y. Cui, Y. Hou, Z. Sun, W. Rao, *ACS Appl. Mater. Interfaces* **2020**, *12*, 14125.
- [15] Y. Gao, H. Li, J. Liu, *PLoS One* **2012**, *7*, e45485.
- [16] Y. Zheng, Q. Zhang, J. Liu, *AIP Adv.* **2013**, *3*, 112117.
- [17] J. W. Boley, E. L. White, R. K. Kramer, *Adv. Mater.* **2015**, *27*, 2355.
- [18] Y. Lin, C. Cooper, M. Wang, J. J. Adams, J. Genzer, M. D. Dickey, *Small* **2015**, *11*, 6397.
- [19] M. G. Mohammed, R. Kramer, *Adv. Mater.* **2017**, *29*, 1604965.
- [20] J.-E. Park, H. S. Kang, J. Baek, T. H. Park, S. Oh, H. Lee, M. Koo, C. Park, *ACS Nano* **2019**, *13*, 9122.
- [21] L. Ren, J. Zhuang, G. Casillas, H. Feng, Y. Liu, X. Xu, Y. Liu, J. Chen, Y. Du, L. Jiang, S. X. Dou, *Adv. Funct. Mater.* **2016**, *26*, 8111.
- [22] L. Wang, J. Liu, *Front. Mater.* **2019**, *6*, 303.
- [23] I. D. Joshipura, H. R. Ayers, C. Majidi, M. D. Dickey, *J. Mater. Chem. C* **2015**, *3*, 3834.
- [24] M. D. Dickey, *ACS Appl. Mater. Interfaces* **2014**, *6*, 18369.
- [25] J. Thelen, M. D. Dickey, T. Ward, *Lab Chip* **2012**, *12*, 3961.
- [26] J. N. Hohman, M. Kim, G. A. Wadsworth, H. R. Bednar, J. Jiang, M. A. LeThai, P. S. Weiss, *Nano Lett.* **2011**, *11*, 5104.
- [27] Y. Lin, J. Genzer, W. Li, R. Qiao, M. D. Dickey, S.-Y. Tang, *Nanoscale* **2018**, *10*, 19871.
- [28] J. Yang, M. A. Cohen Stuart, M. Kamperman, *Chem. Soc. Rev.* **2014**, *43*, 8271.
- [29] M. A. Rahim, S. L. Kristufek, S. Pan, J. J. Richardson, F. Caruso, *Angew. Chem., Int. Ed.* **2019**, *58*, 1904.
- [30] J. H. Ryu, P. B. Messersmith, H. Lee, *ACS Appl. Mater. Interfaces* **2018**, *10*, 7523.
- [31] G. P. Maier, M. V. Rapp, J. H. Waite, J. N. Israelachvili, A. Butler, *Science* **2015**, *349*, 628.
- [32] J. Saiz-Poseu, J. Mancebo-Aracil, F. Nador, F. Busqué, D. Ruiz-Molina, *Angew. Chem., Int. Ed.* **2019**, *58*, 696.
- [33] A. H. Hofman, I. A. van Hees, J. Yang, M. Kamperman, *Adv. Mater.* **2018**, *30*, 1704640.
- [34] H. Lee, B. P. Lee, P. B. Messersmith, *Nature* **2007**, *448*, 338.
- [35] M. A. Rahim, K. Kempe, M. Müllner, H. Ejima, Y. Ju, M. P. van Koevorden, T. Suma, J. A. Braunger, M. G. Leeming, B. F. Abrahams, F. Caruso, *Chem. Mater.* **2015**, *27*, 5825.
- [36] H. Ejima, J. J. Richardson, K. Liang, J. P. Best, M. P. van Koevorden, G. K. Such, J. Cui, F. Caruso, *Science* **2013**, *341*, 154.
- [37] A. Avdeef, S. R. Sofen, T. L. Bregante, K. N. Raymond, *J. Am. Chem. Soc.* **1978**, *100*, 5362.
- [38] M. J. Harrington, A. Masic, N. Holtén-Andersen, J. H. Waite, P. Fratzl, *Science* **2010**, *328*, 216.
- [39] J. H. Park, S. Choi, H. C. Moon, H. Seo, J. Y. Kim, S.-P. Hong, B. S. Lee, E. Kang, J. Lee, D. H. Ryu, I. S. Choi, *Sci. Rep.* **2017**, *7*, 6980.
- [40] M. A. Rahim, M. Björnalm, N. Bertleff-Zieschang, Q. Besford, S. Mettu, T. Suma, M. Faria, F. Caruso, *Adv. Mater.* **2017**, *29*, 1606717.
- [41] T. S. Sileika, D. G. Barrett, R. Zhang, K. H. A. Lau, P. B. Messersmith, *Angew. Chem., Int. Ed.* **2013**, *52*, 10766.
- [42] L. Cademartiri, M. M. Thuo, C. A. Nijhuis, W. F. Reus, S. Tricard, J. R. Barber, R. N. S. Sodhi, P. Brodersen, C. Kim, R. C. Chiechi, G. M. Whitesides, *J. Phys. Chem. C* **2012**, *116*, 10848.
- [43] F. Centurion, M. G. Saborío, F.-M. Allieux, S. Cai, M. B. Ghasemian, K. Kalantar-Zadeh, M. A. Rahim, *Chem. Commun.* **2019**, *55*, 11291.
- [44] M. A. Rahim, G. Lin, P. P. Tomanin, Y. Ju, A. Barlow, M. Björnalm, F. Caruso, *ACS Appl. Mater. Interfaces* **2020**, *12*, 3746.
- [45] M. J. Sever, J. J. Wilker, *Dalton Trans.* **2004**, 1061.
- [46] K. N. Raymond, E. A. Dertz, S. S. Kim, *Proc. Natl. Acad. Sci. USA* **2003**, *100*, 3584.
- [47] B. Kersting, J. R. Telford, M. Meyer, K. N. Raymond, *J. Am. Chem. Soc.* **1996**, *118*, 5712.
- [48] L. Francke, E. Durand, A. Demourgues, A. Vimont, M. Daturi, A. Tressaud, *J. Mater. Chem.* **2003**, *13*, 2330.
- [49] X. Li, M. Li, L. Zong, X. Wu, J. You, P. Du, C. Li, *Adv. Funct. Mater.* **2018**, *28*, 1804197.
- [50] R. Guo, X. Sun, B. Yuan, H. Wang, J. Liu, *Adv. Sci.* **2019**, *6*, 1901478.
- [51] S. Liu, M. C. Yuen, E. L. White, J. W. Boley, B. Deng, G. J. Cheng, R. Kramer-Bottiglio, *ACS Appl. Mater. Interfaces* **2018**, *10*, 28232.
- [52] X. Li, M. Li, J. Xu, J. You, Z. Yang, C. Li, *Nat. Commun.* **2019**, *10*, 3514.
- [53] L. Zhu, B. Wang, S. Handschuh-Wang, X. Zhou, *Small* **2020**, *16*, 1903841.
- [54] M. D. Dickey, *Adv. Mater.* **2017**, *29*, 1606425.
- [55] P. Surmann, H. Zeyat, *Anal. Bioanal. Chem.* **2005**, *383*, 1009.

- [56] W. Zhang, J. Z. Ou, S.-Y. Tang, V. Sivan, D. D. Yao, K. Latham, K. Khoshmanesh, A. Mitchell, A. P. O'Mullane, K. Kalantar-zadeh, *Adv. Funct. Mater.* **2014**, *24*, 3799.
- [57] V. Sivan, S.-Y. Tang, A. P. O'Mullane, P. Petersen, N. Eshtiaghi, K. Kalantar-zadeh, A. Mitchell, *Adv. Funct. Mater.* **2013**, *23*, 144.
- [58] A. L. Suherman, S. Kuss, E. E. L. Tanner, N. P. Young, R. G. Compton, *Analyst* **2018**, *143*, 2035.
- [59] A. L. Suherman, G. Zampardi, H. M. A. Amin, N. P. Young, R. G. Compton, *Phys. Chem. Chem. Phys.* **2019**, *21*, 4444.